**Atmospheric
Chemistry
and Physics**

Aerosol optical properties in the North China Plain during HaChi campaign: an in-situ optical closure study

N. Ma[1], C. S. Zhao[1], A. Nowak[2], T. Müller[2], S. Pfeifer[2], Y. F. Cheng[3], Z.Z. Deng[1], P. F. Liu[1], W. Y. Xu[1], L. Ran[1], P. Yan[4], T. Göbel[2], E. Hallbauer[2], K. Mildenberger[2], S. Henning[2], J. Yu[5], L. L. Chen[5], X. J. Zhou[1,4], F. Stratmann[2], and A. Wiedensohler[2]

[1]Department of Atmospheric and Oceanic Sciences, School of Physics, Peking University, Beijing, China
[2]Leibniz Institute for Tropospheric research, Leipzig, Germany
[3]Center of Global and Regional Environment Research, University of Iowa, Iowa, USA
[4]Key Laboratory for Atmospheric Chemistry, Centre for Atmosphere Watch and Services, Chinese Academy of Meteorological Sciences, China Meteorological Administration, Beijing, China
[5]Wuqing Meteorological Bureau of Tianjin, Tianjin, China

Abstract. The largest uncertainty in the estimation of climate forcing stems from atmospheric aerosols. In early spring and summer of 2009, two periods of in-situ measurements on aerosol physical and chemical properties were conducted within the HaChi (Haze in China) project at Wuqing, a town between Beijing and Tianjin in the North China Plain (NCP). Aerosol optical properties, including the scattering coefficient (σ_{sp}), the hemispheric back scattering coefficient (σ_{bsp}), the absorption coefficient (σ_{ap}), as well as the single scattering albedo (ω), are presented. The diurnal and seasonal variations are analyzed together with meteorology and satellite data. The mean values of $\sigma_{sp,\,550nm}$ of the dry aerosol in spring and summer are 280±253 and 379±251 Mm^{-1}, respectively. The average σ_{ap} for the two periods is respectively 47±38 and 43±27 Mm^{-1}. The mean values of ω at the wavelength of 637 nm are 0.82±0.05 and 0.86±0.05 for spring and summer, respectively. The relative high levels of σ_{sp} and σ_{bsp} are representative of the regional aerosol pollution in the NCP. Pronounced diurnal cycle of σ_{sp}, σ_{ap} and ω are found, mainly influenced by the evolution of boundary layer and the accumulation of local emissions during nighttime. The pollutants transported from the southwest of the NCP are more significant than that from the two megacities, Beijing and Tianjin, in both spring and summer. An optical closure experiment is conducted to better under-

stand the uncertainties of the measurements. Good correlations ($R > 0.98$) are found between the values measured by the nephelometer and the values calculated with a modified Mie model. The Monte Carlo simulation shows an uncertainty of about 30 % for the calculations. Considering all possible uncertainties of measurements, calculated σ_{sp} and σ_{bsp} agree well with the measured values, indicating a stable performance of instruments and thus reliable aerosol optical data.

1 Introduction

Atmospheric aerosols influence the earth's radiation budget directly by scattering and absorbing solar radiation (Charlson et al., 1992), and indirectly by acting as condensation nuclei in cloud formation, thus affecting the optical properties and lifetimes of clouds (Twomey, 1974; Albrecht, 1989; Rosenfeld, 1999, 2000). The radiative forcing of these two effects is estimated at -0.5 W m^{-2} and -0.7 W m^{-2}, respectively, with the largest uncertainty of $+0.8/-1.5$ W m^{-2} among all climate forcing factors (IPCC, 2007). One of the reasons for such great uncertainty is that aerosols have highly inhomogeneous horizontal and vertical distributions (van Donkelaar et al., 2010; Liu et al., 2009) as well as temporal variations, different from well mixed greenhouse gases, such as CO_2 and methane. To better understand the direct effect of aerosols, further knowledge of aerosol optical properties is of critical importance. The aerosol optical properties, e.g., scattering

Correspondence to: C. S. Zhao
(zcs@pku.edu.cn)
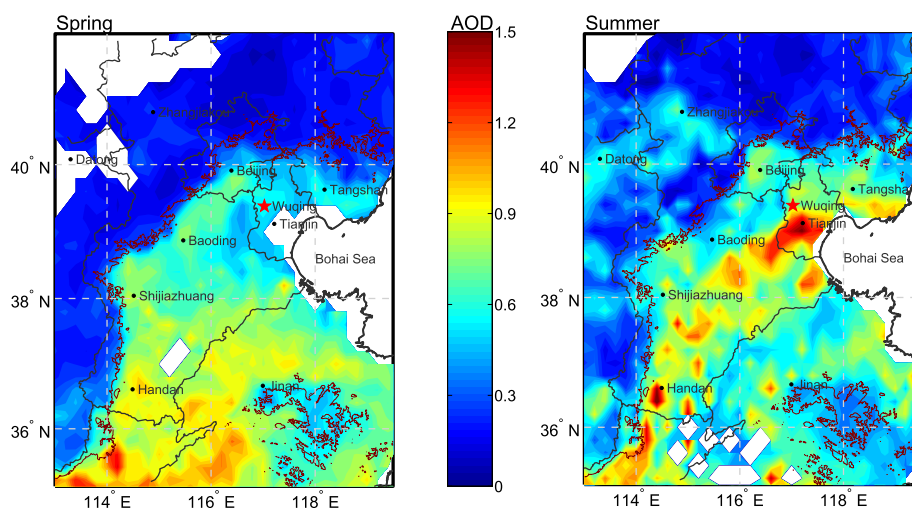
Fig. 1. The map of the NCP. The site is marked as a star. The shaded contour represents the distribution of the MODIS AOD. The dark red dashed denotes the 500 m contour line, which also can be considered as the boundary of the NCP.

coefficient (σ_{sp}), absorption coefficient (σ_{ap}), aerosol optical depth (AOD) and single scattering albedo (ω), are closely related to the aerosol physical and chemical characteristics, which are influenced by many processes, such as aerosol formation, growth and removal. To estimate the aerosol optical properties and radiative impacts with the measured physical and chemical characteristics, the Mie model and radiative transfer models are widely employed. However, due to the uncertainties in measurements and models, the calculations are needed to be evaluated (Quinn et al., 1998; Bond et al., 1998; Sheridan et al., 2001). Therefore, more investigations on aerosol optical properties and optical closure studies are urgently needed especially in regions such as Asia, Africa, and South-America.

Closure studies are usually used for estimating the uncertainties of measurement techniques and numerical models. Quinn et al. (1996) reviewed some of the closure studies in the research of aerosols. A typical closure study requires an over-determined set of observations. Then a comparison between a measured value of an important system property and a value calculated with an appropriate model based on independent measurements can be made. Closure is achieved if there is an agreement between these two values within the accepted level of uncertainty (Quinn et al., 1998). Closure studies can be used as an examination of the measurements and models. It also provides a platform for sensitivity studies as well as an approach to evaluate and reduce the uncertainties of both measurements and models. Some optical closure studies were already done in the past decades (e.g. Wex et al., 2002; Cheng et al., 2007; Cheng et al., 2009; Pesava et al., 2001)

Along with the rapid growth of population and economy in China, emissions of anthropogenic pollutants increased dra-

matically in the past several decades. Urbanization and industrial activities produce large amounts of aerosols, especially in the North China Plain (NCP). Aerosol optical properties in China are highly complex and differ from those in Europe or North America (Höller et al., 2003). Moreover, the widespread consumptions of coal and biomass fuels make China a significant source region of black carbon (BC). It was reported that the BC amount emitted in China was around one fourth of the global anthropogenic BC emissions (Cooke et al., 1999; Street et al., 2001; Bond et al., 2004). In the past decade, there were some studies focusing on aerosol optical properties (Yan et al., 2008; Xu et al., 2002, 2004; Cheng, 2008a, 2009), but only a few studies touched the uncertainty evaluation of measured aerosol properties and related models (Cheng et al., 2007).

In this paper, the results of aerosol optical property observations during a two-period in-situ measurement campaign at a site in the north of NCP are presented. The characteristics of aerosol optical properties are analyzed. An aerosol optical closure study between measured and calculated aerosol scattering coefficients and the related uncertainty evaluation are shown.

2 Measurements

2.1 The field site

The data used in this study was collected during the HaChi (Haze in China) campaigns. Measurements of aerosol optical, chemical, hygroscopic properties and size distribution, as well as trace gas observations, were conducted in Wuqing in the north NCP in two periods of 2009: the spring campaign was from 6 March to 5 April (65–95 DOY); while the

summer campaign was from 12 July to 14 August (193–226 DOY).

The map of the NCP is shown in Fig. 1. The population is dense and the land use is mainly agricultural in the NCP. Several large cities with rapidly developing economy and industry are located in the NCP. Wuqing (marked as a star in Fig. 1) is a town with about 0.8 million inhabitants, located between two megacities: Beijing (16 million inhabitants, 80 km away from Wuqing) and Tianjin (10 million inhabitants, 30 km away from Wuqing), in the north of the NCP. The site is located in the suburban area of Wuqing and thus representative of the regional anthropogenic aerosol pollution.

An automatic weather station (AWS) is located next to the aerosol measurement containers. During the whole campaigns, meteorological parameters, such as wind speed, wind direction, relative humidity (RH) and temperature (T) were measured continuously and reported as 1-min data. The weather conditions were either clear or cloudy during the spring campaign, and no precipitation event occurred; while there were 10 rain events in the summer campaign. In both of the two periods, the wind direction was dominated of southwest, with average wind speeds of 3.2±2.2 m/s and 1.8±1.2 m/s, respectively. T and RH show an evident diurnal cycles (Fig. 2). Average T and RH are 7.8±5.6 °C and 42.2±20.7 % in spring, 26.3±3.4 °C and 75.4±15.3 % in summer, respectively.

Most of the ground-based measurements were conducted in a measurement container, in which the temperature was maintained at 22 °C. The sample air was collected with a PM_{10} inlet (16.67 L/min) installed on the top of a stainless steel tube with a diameter of 3/4 inch and 7 m above the ground level. The sample air was split into several flows inside the container, passing through stainless steel tubing, to different instruments. The residence time for the sample air in the inlet line was about 5 s. An automatic aerosol diffusion dryer (Tuch et al., 2009) was set upstream all of the instruments, to keep the RH of the sample air below 30 %.

2.2 Nephelometer measurements

The σ_{sp} and σ_{bsp} for dry aerosols were measured by a total/back integrating nephelometer at wavelengths of 450, 550 and 700 nm (TSI, Inc., Shoreview, MN USA, Model 3563; Heintzenberg and Charlson, 1996; Anderson et al., 1996, 1998). The temporal resolution of the measurement was 1 min. However, in this study, 10-min averaged data was used. The nephelometer was calibrated before each of the two campaigns using CO_2 (Anderson et al., 1996). Particle free air checks were performed once a day. The truncation and non-Lambertian error was corrected using a modified Mie model, which applied in the closure study. The correction factor is defined as:

$$C = \frac{\sigma_{sp/bsp,Mie}}{\sigma_{sp/bsp,Modified-Mie}} \qquad (1)$$
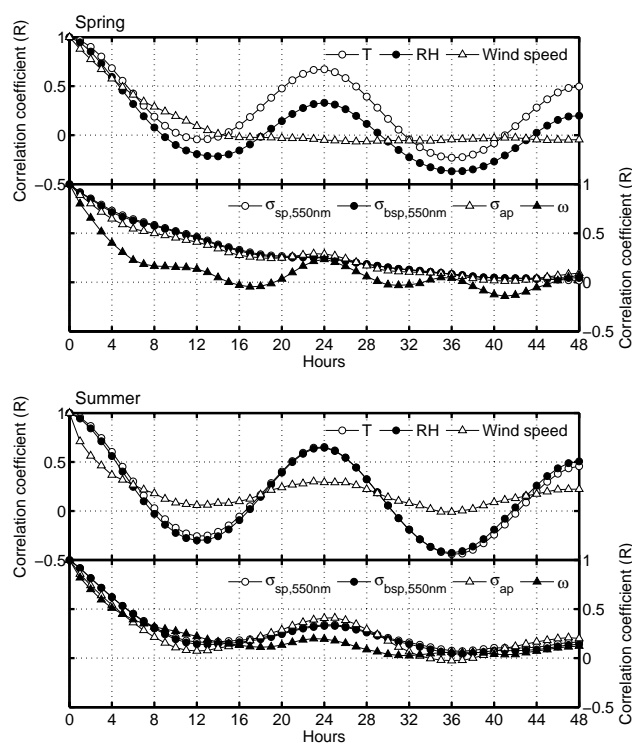
Fig. 2. Autocorrelation analysis of the meteorological parameters and the aerosol optical properties.

Where $\sigma_{sp/bsp,Mie}$ is the ideal scattering or hemispheric backscattering coefficient of dry aerosols calculated with the Mie theory, while $\sigma_{sp/bsp,Modified-Mie}$ is calculated with the Modified Mie model simulating the nephelometer. The calculations are based on measured particle number size distributions (PNSDs) and the black carbon (BC) concentrations. The details will be described in Sect. 3.

2.3 MAAP measurements

A Multi-angle Absorption Photometer (MAAP Model 5012, Thermo, Inc., Waltham, MA USA) was employed to determine the σ_{ap} for dry particles. The instrument determines σ_{ap} via the simultaneous measurement of light (637 nm) passing through its filter and scattered back from particles accumulated on it. It operates at two detection angles to resolve the influence of light-scattering aerosol components on the angular distribution of the back-scattered radiation (Petzold and Schönlinner, 2004). The MAAP provides the BC mass concentrations in unit of μg/m³. According to the manual, σ_{ap} at 637 nm can be calculated with $\sigma_{ap} = m_{BC} \cdot 6.6 \, m^2/g$, where m_{BC} is the mass concentration of BC. The mass absorption efficiency of 6.6 m²/g has been validated by the comparison between the impactor-derived elemental carbon mass concentration and the MAAP measurements. The sampling frequency was 1 min, and 10-min averaged data was used.

2.4 TDMPS/APS measurements

A Twin Differential Mobility Particle Sizer (TDMPS, IfT, Leipzig, Germany; Birmili et al., 1999) was used to measure PNSDs with electrical mobility diameter from 3 to 800 nm. An Aerodynamic Particle Sizer (APS Model 3320, TSI, Inc., Shoreview, MN USA) was employed to measure PNSDs with aerodynamic diameter from 0.5 to 10 μm. Both of them were operated under dry conditions. It took 10 min for a complete scan for both TDMPS and APS. A series of processing was applied to the TDMPS data. Following the procedure described by Wiedensohler et al. (1997), the counting efficiencies of CPC (TSI 3010) and UCPC (TSI 3025) were measured beforehand. Inversion of the raw data was done according to an algorithm introduced by Stratmann and Wiedensohler (1996). Electrical mobility diameters measured by TDMPS and aerodynamic diameters measured by APS were converted to volume equivalent diameter (DeCarlo et al., 2004), using a density of $1.7\,\text{g\,cm}^{-3}$ for the particles larger than 800 nm as a mean density for the coarse mode (Wehner et al., 2008). Then the PNSDs measured by TDMPS and APS were combined to yield aerosol size distributions with diameter range from 3 nm to 10 μm. Furthermore, the PNSD data was corrected for diffusion losses, gravitational losses and impaction losses in the sampling tubing. The electrostatic losses were ignored, since conductive tubing was used in all portions of the inlet system.

3 Method of optical closure for dry aerosols

An optical closure for dry aerosols is carried out to better understand the dependence of aerosol optical properties on their physical and chemical characterizations, and to evaluate the quality of the measurements.

A two-component optical aerosol model (Wex et al., 2002; Cheng et al., 2006) was used for dry aerosol optical closure. In this model, aerosol species are divided into light-absorbing BC and non-light-absorbing components such as sulfate, nitrate, ammonium, OC and other undetermined ones, since σ_{sp} is not sensitive to the mass fraction of these non-light-absorbing components (Wex, 2002).

To obtain the size-resolved volume fraction of BC, the average BC mass size distribution observed during the Campaigns of Air Quality Research in Beijing and Surrounding Region 2006 (CAREBeijing-2006; Cheng et al., 2009) was used in this study. In Cheng's work, size-resolved BC mixing states were measured by a Volatility Tandem Differential Mobility Analyzer (VTDMA) at the regional site Yufa in the south of Beijing during the summer of 2006. Both of Yufa and Wuqing are located in the megacity cluster of Beijing and Tianjin. The two sites, about 60 km away from each other, have similar surroundings and pollution levels. Both of them are located in suburban areas and are influenced mainly by the regional pollution transported from the southern industri-

alized regions. Thus, the BC mass size distribution normalized by the total mass concentration in Wuqing is assumed to be the same as the average one in Yufa, which follows a quasi-log-normal distribution with a geometric mean diameter of 114 nm and a standard deviation of 2.12. The BC mass concentration at a given particle size and time can be calculated with the following equation:

$$m\left(\log D_p, t\right)_{\text{Wuqing,BC}} = \tag{2}$$

$$\frac{m\left(\log D_p\right)_{\text{Yufa,ext}-\text{BC,ave}} + m\left(\log D_p\right)_{\text{Yufa,int}-\text{BC,ave}}}{\sum\limits_{\log D_p}\left(m\left(\log D_p\right)_{\text{Yufa,ext}-\text{BC,ave}} + m\left(\log D_p\right)_{\text{Yufa,int}-\text{BC,ave}}\right)} \cdot$$

$$m\left(t\right)_{\text{Wuqing,MAAP}}$$

Where, $m\left(\log D_p\right)_{\text{Yufa,ext}-\text{BC,ave}}$ represents the average mass concentration of externally mixed BC in size bin D_p measured at Yufa, while $m\left(\log D_p\right)_{\text{Yufa,int}-\text{BC,ave}}$ is the average mass concentration of internally mixed BC at D_p. $m\left(t\right)_{\text{Wuqing,MAAP}}$ is the total mass concentration of BC measured by MAAP at Wuqing.

In other words, only the normalized BC mass size distribution measured at Yufa was used here. The BC total mass concentrations were kept the same as the values derived from the MAAP measurements at Wuqing. The BC volume fraction at each size is calculated as:

$$f\left(\log D_p\right)_{\text{BC,V}} = \frac{m\left(\log D_p, t\right)_{\text{Wuqing,BC}}}{\rho_{\text{BC}} \cdot V\left(\log D_p, t\right)_{\text{Wuqing,total}}} \tag{3}$$

Where, $V\left(\log D_p, t\right)_{\text{Wuqing,total}}$ is the volume concentration of sampled aerosols in size bin D_p derived from TDMPS and APS, and ρ_{BC} is the density of BC.

In literature (Sloane et al., 1983, 1984; Sloane and Wolff, 1985; Sloane et al., 1991; Ouimette and Flagan, 1982; Seinfeld and Pandis, 1998), the density of BC is reported as a range from $1.00\,\text{g/cm}^3$ to $2.00\,\text{g/cm}^3$. Accordingly, an average value of $1.5\,\text{g/cm}^3$ is used, and the uncertainty (3σ) is assigned to be 33 % covering the possible range.

Lacking measurements of BC mixing state, a completely external mixture and internal mixture of BC are assumed for the two-component optical aerosol model. Because atmospheric aerosols are probably partial combination of internally and externally mixed particles (Wex, 2002; Chandra et al., 2004), the $\sigma_{\text{sp}}(\sigma_{\text{bsp}})$ measured by nephelometer should be within the range determined by the calculated values based on the assumption of external mixture and internal mixture of BC.

For the case of completely external mixture, the PNSDs of BC and non-absorbing component are obtained by multiplying the aerosol PNSDs with $f(\log D_p)_{\text{BC,V}}$ and $1 - f(\log D_p)_{\text{BC,V}}$, respectively. The refractive index used for BC component is $\tilde{m}_{\text{BC}} = 1.96 - 0.66i$ (Seinfeld and Pandis, 1998), and for non-absorbing component it is set to $\tilde{m}_{\text{non}} = 1.53 - 10^{-7}i$ (Wex et al., 2002).

For a completely internally mixed aerosol, the BC is considered to be homogeneously mixed with non-absorbing component with the size dependent volume fraction $f(\log D_p)_{BC,V}$. The refractive index is derived as a volume-weighted average between the two components:

$$\tilde{m}(\log D_p) = f(\log D_p)_{BC,V}\,\tilde{m}_{BC} + \left(1 - f(\log D_p)_{BC,V}\right)\tilde{m}_{non} \quad (4)$$

The refractive indices $\tilde{m}$ are size dependent, due to the size dependence of $f(\log D_p)_{BC,V}$.

Based on the Mie theory (Mie, 1908), the scattering efficiency Q_{sp} and hemispheric back scattering efficiency Q_{bsp} can be calculated by integrating the scattering intensity function $|S(\theta, x, \tilde{m})|$ from 0° to 180° and from 90° to 180°, respectively:

$$Q_{sp,bsp} = \frac{1}{x^2}\int_{\theta} |S(\theta, x, \tilde{m})|^2 \sin\theta d\theta \quad (5)$$

where, $x = \pi D_p/\lambda$. D_p is the volume equivalent diameter of particles. λ is the wavelength of light, and θ is the scattering angle.

Different from the scattering angle ranges used in the original Mie model, the scattering integration angle of TSI 3563 integrating nephelometer ranges from 7° to 170° for scattering and from 90° to 170° for hemispheric back scattering, respectively. Thus, the measured values are truncated in the near-forward and near-backward angular ranges. Furthermore, the light source of the nephelometer is not strictly Lambertian and shows a non-ideal angular response (Anderson et al., 1996). These two factors account for the main systematic errors of the nephelometer measurements and these two effects must be corrected.

The angular response is solved in the Mie calculations based on the Bohren-Huffman Mie model (BHMIE) (Bohren and Huffman, 1983). The $\sin\theta$ term in Eq. (5) is replaced by the angular sensitivity curves $f(\theta)_{sp}$ and $f(\theta)_{bsp}$, derived from a calibration experiment of the TSI 3563 nephelometer (Anderson et al., 1996). The σ_{sp} and σ_{bsp} are calculated as:

$$\sigma_{sp,bsp} = \int_{D_p}\left[\frac{1}{x^2}\int_{\theta}|S(\theta, x, \tilde{m})|^2 f(\theta)_{sp,bsp}d\theta\right]\cdot \quad (6)$$
$$\left(\frac{\pi}{4}D_p^2\right)\cdot N(\log D_p)\cdot d\log D_p$$

Where, $N(\log D_p)$ is the PNSD.

The modified Mie model introduced above, which simulates the measurements of TSI 3563 nephelometer, is applied in the correction of nephelometer measurements and the optical closure for dry particles. Comparisons between the calculated σ_{sp} (σ_{bsp}) and the values measured by nephelometer are shown in Sect. 4.2.

4 Results and discussion

4.1 Measurements of aerosol optical properties

4.1.1 Overview

Table 1 summarizes the statistics on measured aerosol optical properties during the two campaigns. For 550 nm, the mean σ_{sp} for the spring campaign and the summer campaign are 280 ± 253 and $379\pm251\,\mathrm{Mm}^{-1}$, respectively. The mean σ_{ap} of the two campaigns are 47 ± 38 and $43\pm27\,\mathrm{Mm}^{-1}$, respectively.

The σ_{sp} in Wuqing is lower than the mean value of Beijing ($488\pm370\,\mathrm{Mm}^{-1}$) in June, 1999, while the σ_{ap} is half of that in Beijing ($83\pm40\,\mathrm{Mm}^{-1}$) (Bergin et al., 2001). During January 2005, the σ_{sp} and σ_{ap} in Beijing had been found to be at an even higher level of 777 ± 689 and $89\pm74\,\mathrm{Mm}^{-1}$, respectively (J. Heintzenberg, personal communication, 2008).

Compared with the regional sites around Beijing, the σ_{sp} and σ_{ap} in Wuqing are about twice as much as the mean values measured in Shangdianzi regional background station (SDZ) (175 ± 189 and $18\pm13\,\mathrm{Mm}^{-1}$) during 2003 to 2005 (Yan et al., 2008). Garland et al. (2009) reported a mean σ_{sp} of $361\pm295\,\mathrm{Mm}^{-1}$ and a mean σ_{ap} of $52\pm37\,\mathrm{Mm}^{-1}$ measured in Yufa in summer of 2006. They are very similar to the values observed in Wuqing.

Compared with other regional sites in China, the σ_{sp} in Wuqing is similar to that in Lin'an ($353\pm202\,\mathrm{Mm}^{-1}$) in November 1999 (Xu et al., 2002) and in Xinken, China ($333\pm137\,\mathrm{Mm}^{-1}$) in October 2004 (Cheng et al., 2008a). The σ_{ap} in Wuqing is a factor of 0.6 lower than that in Xinken ($70\pm42\,\mathrm{Mm}^{-1}$), while it is the double of that measured in Lin'an ($23\pm14\,\mathrm{Mm}^{-1}$). Overall, the σ_{sp} and σ_{ap} in Wuqing are higher than that in the rural area and lower than that measured in megacities.

For seasonal comparison, the average σ_{sp} and σ_{bsp} are higher in summer than in spring, while the average σ_{ap} shows an opposite variation. This is mainly due to the seasonal changes of air pollutant transportation. The change of local pollutant emissions is also one potential reason. Details will be discussed in Sects. 4.1.2 and 4.1.3.

The single scattering albedo, defined as $\omega = \sigma_{sp}/(\sigma_{sp}+\sigma_{ap})$, is one of the most important parameters in estimating the direct aerosol radiative forcing. Even a small error in its estimation might change the sign of the aerosol radiative forcing (Takemura et al., 2002). To calculate ω at the wavelength of 637 nm, a wavelength correction is applied to the measured σ_{sp} using an empirical approach, $\sigma_{sp} \propto \lambda^{\alpha}$. The Ångström exponent (α) is yielded from the measured σ_{sp} at the wavelength of 550 nm and 700 nm.

The average ω at the wavelength of 637 nm in Wuqing is 0.82 ± 0.05 in spring and 0.86 ± 0.05 in summer, respectively. These values are similar to those measured in Yufa, which is 0.86 ± 0.07 at the wavelength of 532 nm (Garland et al., 2009). Yan et al. (2008) reported a higher ω in spring

Table 1. Statistic values of aerosol optical properties measured at dry condition. (4321 data points for spring campaign and 4897 data points for summer campaign).

		Mean		Std		Median	
		spring	summer	spring	summer	spring	summer
σ_{sp} (Mm^{-1})	450 nm	363	464	319	290	280	392
	550 nm	280	379	253	251	206	314
	700 nm	191	270	175	191	137	218
σ_{bsp} (Mm^{-1})	450 nm	54	60	43	37	44	51
	550 nm	45	49	37	31	35	42
	700 nm	36	41	27	26	27	34
σ_{ap} (Mm^{-1})	637 nm	47	43	38	27	34	37
L_V (km)	550 nm	–	4.2	–	4.1	–	4.2
ω	637 nm	0.82	0.86	0.05	0.05	0.82	0.87
b (%)	550 nm	17	13	2	1	17	13
$\mathring{A}$	450–700 nm	1.45	1.33	0.34	0.24	1.52	1.32

(0.91±0.03) and a lower ω in summer (0.86±0.06) in SDZ. The ω in Wuqing is relatively low compared to the values retrieved through the Aerosol Robotic Network (AERONET) for the northern hemisphere (0.85–0.95) (Dubovik et al., 2002), since our measurements are controlled at a RH below 30 %. At ambient condition, water uptakes of aerosols would result in higher ω (Cheng et al., 2008b).

The average ω in spring is lower than that in summer, caused by higher emissions of BC in spring than in summer (Zhang et al., 2009; Lu et al., 2010). In northern China, house heating in early spring is provided by central heating plants, mainly fueled by coal. Aerosols with a relative high fraction of soot from combustion processes are emitted into the atmosphere.

4.1.2 Wind dependence of aerosol optical properties

Figure 3 presents the wind dependence of the σ_{sp}, σ_{ap} and ω. From the wind rose (Fig. 3a and e), it can be found that the prevailing winds came from SSW for both spring and summer campaign. In spring, weather systems with strong winds in NNW direction occurred occasionally.

The average MODIS (Moderate Resolution Imaging Spectroradiometer) AOD distributions at the NCP during the two campaign periods are presented in Fig. 1. The AOD, which represents the columnar optical property of aerosols at ambient condition, is influenced by many factors such as the vertical profiles of RH and PNSD. However, it can provide information about the distribution of regional aerosol pollution, which can help to understand the wind dependence pattern of aerosol optical properties.

In both spring and summer, the average σ_{sp} and σ_{ap} (dash-dot line) for southerly winds (90°-270°) are higher than that for northerly winds, caused by the transportation of pollutants from the southern areas. This can be seen through the AOD distributions in Fig. 1. In both spring and summer, the

AOD of the southern areas is obviously higher than that of the northern areas. Since in the NCP, the major cities and industrial areas with high pollution emissions are mainly located in the southern region.

In spring, the maximum σ_{sp} and σ_{ap} occur with calm winds (wind speed <2 m s^{-1}), independent of wind direction. This indicates that aerosol emissions of local sources mostly contribute to the aerosol pollution. It should be noticed that the average AOD in Beijing is higher than in the areas around the city. But the NW wind, which is from the direction of Beijing, does not cause high σ_{sp} and σ_{ap}. The reason is that in spring the NW winds usually occur with cold front systems and with high wind speeds. The dilution effect of such strong winds is more significant. The strong northerly winds sweep away air pollutants, resulting in the low σ_{sp} and σ_{ap} in spring.

In summer, the maximum σ_{sp} and σ_{ap} occur with southerly winds, relating to the pollutants transportation from the southern region in the NCP, as shown in Fig. 1.

The wind maps of ω are shown in Fig. 3 d and h. In both spring and summer, the ω accompanied by calm winds is always lower than during strong winds, indicating that the locally emitted aerosols contain a higher fraction of BC than the aerosols transported from surrounding areas. During transport, the aging process and secondary aerosol formation produce non-light-absorbing components. As indicated in Cheng et al. (2009), for aged aerosols, even though the coating effect may increase the light absorption of the BC, the scattering increase by the secondary particle formation and condensation will still overcome the increase of the light absorption, which will result in an increase of ω. The average ω for southerly winds is lower than that for northerly winds, which may relate to the denser industrialization in the south of the NCP.
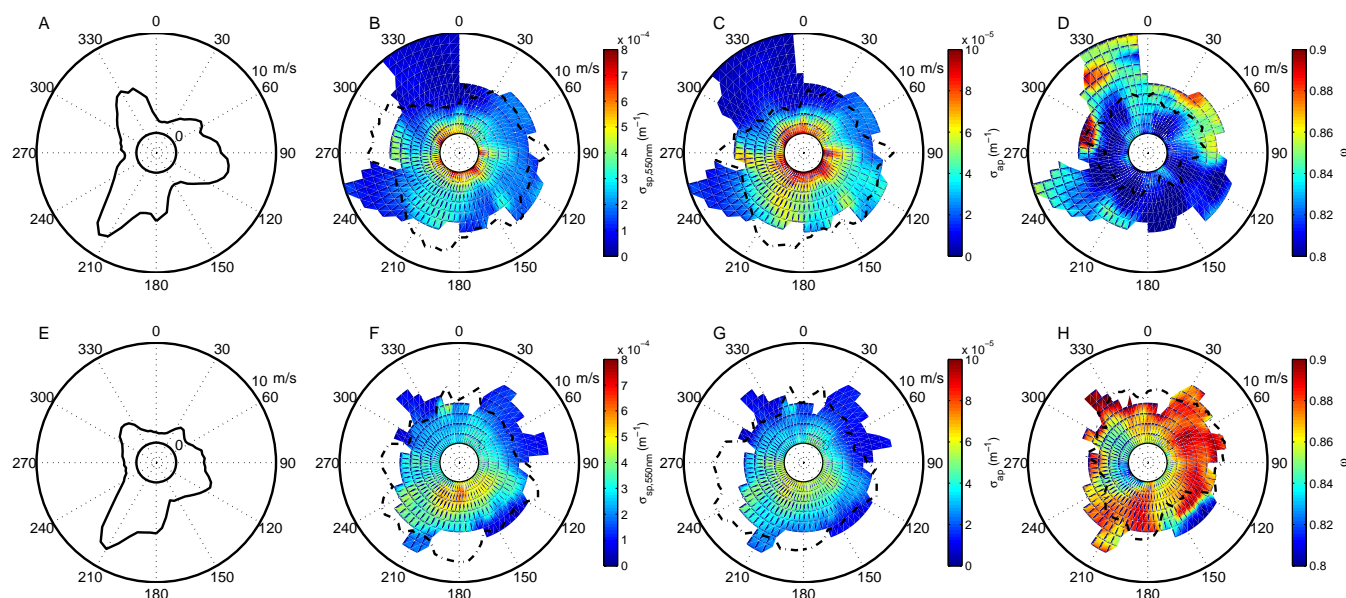
Fig. 3. Wind speed and direction dependence map of σ_{sp} **(B, F)**, σ_{ap} **(C, G)** and ω **(D, H)**, as well as wind rose **(A, E)**. The upper fours pictures are for spring and the lower ones are for summer. In each picture, the shaded contour indicates the average of variables for varying wind speeds (radial direction) and wind directions (transverse direction). The dash-dot lines stand for the relative mean values at each wind direction.

4.1.3 Diurnal variation of aerosol optical properties

Figure 4 shows the average diurnal cycle of the wind speed, σ_{sp}, σ_{ap} and ω during the spring and summer campaign. Evident diurnal variations can be found for all of those variables, mainly determined by the diurnal cycle of the boundary layer height and the local emission pattern. The diurnal cycle of wind speed and secondary aerosol production are also potential players.

The diurnal patterns of the σ_{sp} and σ_{ap} are similar in spring and summer. The maximum of the σ_{sp} and σ_{ap} appears in the morning between 06:00 LT and 08:00 LT. During this period, the rapid increase of the aerosol pollutants is mainly due to the morning traffic, just before the increase of the boundary layer height. The dilution effect of the increasing boundary layer height results in a decrease of the σ_{sp} and σ_{ap} between 08:00 LT and 14:00 LT. They reach their minimum around 16:00 LT. During night, the σ_{sp} and σ_{ap} remain at relative high values, since particle emissions are accumulated in the shallow nocturnal boundary layer.

The σ_{sp} and σ_{ap} are lower in spring than in summer during night. This difference is mainly caused by the different levels of wind speed between spring and summer at night. The diurnal pattern of wind speed is shown in Fig. 4. The wind speed during the nighttime in spring (approximately 3 m/s) is higher than that in summer (around 1.5 m/s). The higher average wind speed in springtime suppresses accumulation of pollutants at ground level at night.

The diurnal pattern of ω shows two dips, first in the morning and again in the evening probably caused by the emission of diesel engine trucks, since trucks are forbidden to enter the city area of Wuqing during the daytime of 08:00 LT–20:00 LT. The maximum ω appears around 14:00 LT. During the daytime, the light-scattering aerosols are enhanced by secondary aerosol formation and aging processes, which rapidly occur in the NCP (Wu et al., 2007; Wiedensohler et al., 2009). This could be the potential explanation for the maximum ω in the afternoon.

The median values (dash) of all aerosol optical properties are typically different from the mean values (dot), since the probability distributions of these variables are deviate from normal distributions. For σ_{sp} and σ_{ap}, the median values are lower than the arithmetic mean values, especially in spring campaign, indicating heavier pollution events in spring than in summer.

4.1.4 Aerosol optical properties in pollution episodes

Time series of the measured optical properties for the PM_{10} aerosols at dry condition (RH<30 %) are presented in Fig. 5. In both spring and summer, large temporal variations can be found for all optical properties mainly relating to the changing of weather systems. Some heavy pollution events can be identified. A pollution episode is defined as a significant rise in σ_{sp} and σ_{ap}, satisfying that both of σ_{sp} and σ_{ap} are within the top 20 % highest values with lasting time of at least 12 h. We determined three episodes in spring and two in summer campaign, respectively, as shown in Fig. 5.

Table 2. The fitting parameters (b) and correlation coefficients (R) of the linear fittings for calculated and measured σ_{sp}, σ_{bsp} and σ_{ap}.

λ	spring		summer	
	external	internal	external	internal
	σ_{sp}			
450 nm	1.12 (0.987)	0.97 (0.986)	0.896 (0.989)	0.780 (0.990)
550 nm	1.13 (0.987)	1.02 (0.986)	0.913 (0. 989)	0.827 (0. 990)
700 nm	1.15 (0.987)	1.08 (0.987)	0.945 (0. 989)	0.889 (0. 990)
	σ_{bsp}			
450 nm	0.817 (0.985)	0.646 (0.982)	0.743 (0.991)	0.575 (0.988)
550 nm	0.839 (0.986)	0.706 (0.984)	0.775 (0.991)	0.642 (0.990)
700 nm	0.850 (0.987)	0.754 (0.986)	0.759 (0.988)	0.668 (0.989)
	σ_{ap}			
637 nm	0.705 (1.00)	1.63 (0.997)	0.705 (1.00)	1.71 (0.996)
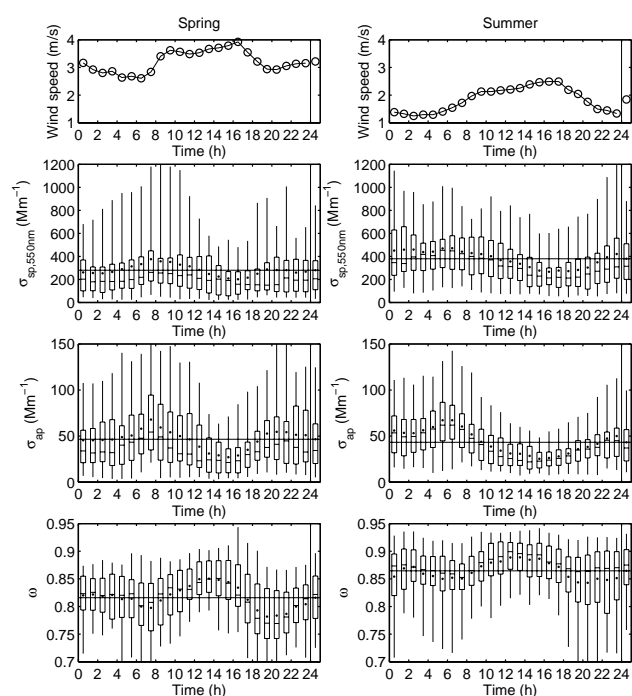
Fig. 4. The average diurnal cycle of wind speed, σ_{sp}, σ_{ap} and ω. The left 4 pictures are for spring and the right ones are for summer. In each picture, the boxes and whiskers denote the 5, 25, 50, 75 and 95 percentiles, while the dots denote the mean values. The x-axis denotes the time of day, with the last box-and-whisker denoting the percentile and mean value for the entire period. The horizontal line also denotes the mean value for the entire study period.

For the episodes in spring, the average $\sigma_{sp,550\,nm}$ and σ_{ap} are 742 ± 283 Mm^{-1} and 112 ± 37 Mm^{-1}, respectively, which are about two times higher than the average values for the whole campaign. The average ω is 0.84 ± 0.03, 2.4 % higher than that of the whole period. The prevailing winds dur-

ing these episodes are mainly from SSW and ESE, basically same as the prevailing winds for the whole period. Because there is infrequent strong wind from the NW, the average wind speed for the episodes (1.7 ± 1.2) is much less than that for the whole period (3.2 ± 2.2). It seems that these episodes in spring occurred in stable weather systems. The accumulation of locally emitted aerosols causes the relative high σ_{sp} and σ_{ap}, and aging processes cause the high ω (Cheng et al., 2009).

For the episodes in summer, the average $\sigma_{sp,550\,nm}$ and σ_{ap} are 874 ± 282 Mm^{-1} and 85 ± 26 Mm^{-1}, respectively. The average ω is 0.89 ± 0.03, 3.5 % higher than that of the whole period. The winds during these episodes are from S and SSW, with the average wind speed of 1.8 ± 0.6, close to the average value of the whole period (1.8 ± 1.2). The episodes in summer are all caused by the advection of air pollutants from the southern regions under the southerly winds from consecutive synoptic weather patterns.

4.2 Optical closure for dry particles

4.2.1 Comparison of measured and calculated optical properties for dry particles

For the optical closure of the dry PM$_{10}$ aerosols, comparisons between measured and calculated σ_{sp} and σ_{bsp} were performed for both of the spring and summer datasets. As described in Sect. 3, σ_{sp} and σ_{bsp} were calculated based on the combined PNSDs measured by TDMPS and APS. A modified Mie model was applied for simulating the measurements of nephelometer. Calculations were carried out for the wavelengths of 450, 550 and 700 nm corresponding to the wavelengths of TSI 3563 integrating nephelometer. Based on the two-component optical aerosol model, either completely external or internal aerosol mixing states were assumed to define the refractive indices.
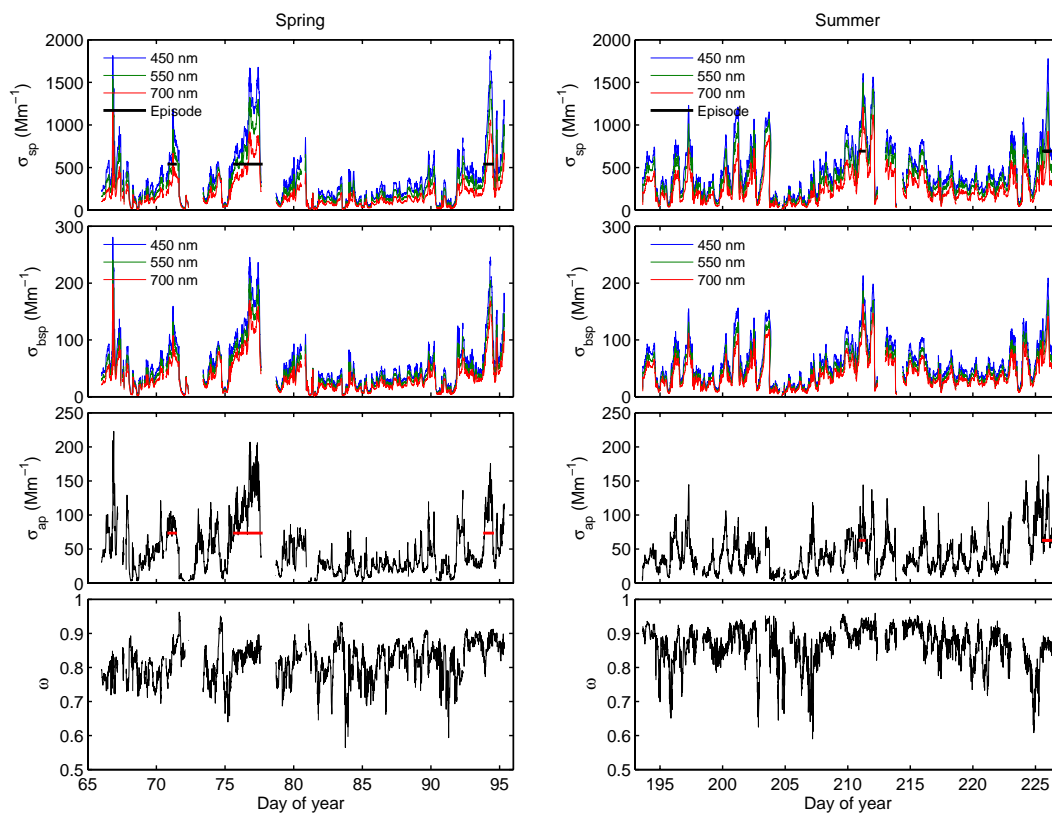
Fig. 5. Time series of measured σ_{sp}, σ_{bsp}, σ_{ap} and ω in spring and summer campaign. The horizontal short lines denote the episodes.
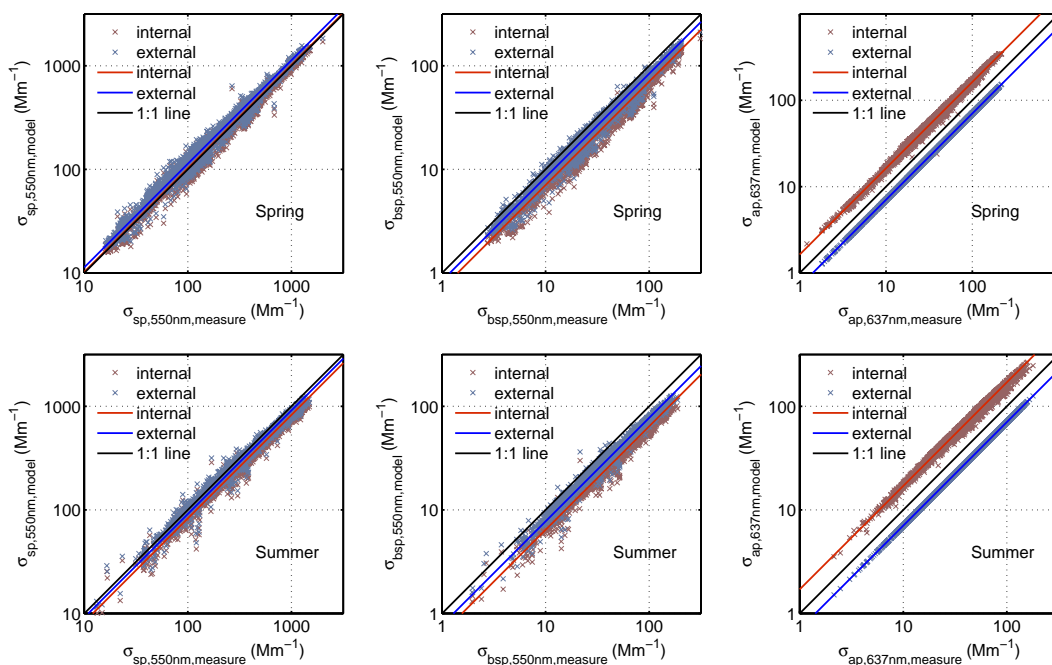
Fig. 6. Comparisons of measured and calculated σ_{sp}, σ_{bsp} and σ_{ap} in log-scale coordinates, including the 1:1 reference lines. For σ_{sp} and σ_{bsp}, only the results at 550 nm are shown. The straight lines represent the linear regression fittings to the data.

The σ_{ap} was also calculated for 637 nm using the model, data, and mixing states mentioned above. The result was compared to the σ_{ap} measured by MAAP. This comparison is not a true closure study, since the MAAP-derived BC mass concentration is also used in the model to calculate σ_{ap}.

Measured σ_{sp} (σ_{bsp}) versus calculated $\sigma_{sp}(\sigma_{bsp})$ at the wavelength of 550 nm and measured σ_{ap} versus calculated σ_{ap} at the wavelength of 637 nm are shown for both campaign periods in Fig. 6. In general, the σ_{sp} and σ_{bsp} calculated for external mixture are slightly larger than that for internal mixture. For wavelengths of 450, 550 and 700 nm, the $\sigma_{sp,external}$ are respectively factors of 1.14, 1.10 and 1.06 larger than the $\sigma_{sp,internal}$, while the $\sigma_{bsp,external}$ are respectively factors of 1.26, 1.19 and 1.13 larger than the $\sigma_{bsp,internal}$. However, the σ_{ap} calculated for internal mixture is much larger than that for external mixture, as a factor of 2.32. This is because for external mixture, only BC particles make contribution to absorption; while for internal mixture, BC is dispersed in all particles leading to the well-known enhancement of absorption. For the same BC concentration, internally mixed particles have a larger absorbing cross section than externally mixed particles (Jacobson, 2000; Cheng, 2007). This result is in a good agreement with the studies of Cheng et al. (2006). Wex et al. (2002) reported a lower factor, which is 2.05, at a European site.

To quantify the comparison of measured and calculated values, linear fitting was applied for σ_{sp}, σ_{bsp} and σ_{ap}. We assume that the relationship between calculated and measured values is $\sigma_{model} = b \cdot \sigma_{measure}$. Since the values spread over 3 orders of magnitudes, if the fitting is done in linear coordinates, the large values will be overrepresented. Therefore, the fitting formula is modified as $\log(\sigma_{model}) = \log(b) + \log(\sigma_{measure})$ to yield more reasonable results.

Table 2 summarizes the fitting parameters (b) and the correlation coefficients (R) for σ_{sp}, σ_{bsp} and σ_{ap}. It can be noted that for both campaign periods, measured values and calculated values have significant correlations. At all of the three wavelengths, the correlation coefficients are above 0.98. The fitting parameters b are all around 1 for the three wavelengths.

As mentioned above, atmospheric aerosols are partial combinations of internal and external mixtures, due to their sources, physical and chemical processes, and stage of mixing state. The measured values should fall within the range limited by the calculated values for internal and external mixture.

It should be noticed that only a small part of the nephelometer-measured σ_{sp} and σ_{bsp} fall within the range of the corresponding calculated values based on the assumptions of internal and external mixture. Table 3 shows the ratios of the amount of measured σ_{sp} and σ_{bsp} that fall within the two calculated values to the total amount of the measured σ_{sp} and σ_{bsp}. Most of the ratios are low, varying from 1.6 % to 84.4 % for different wavelengths and parameters. Discrep-

Table 3. The ratios of the amount of nephelometer-measured σ_{sp} and σ_{bsp} that fall within the range of the corresponding calculated values based on the assumptions of internal and external mixture to the total amount of the measured values.

λ	σ_{sp}		σ_{bsp}	
	spring	summer	spring	summer
450 nm	84.4 %	46.2 %	13.1 %	1.4 %
550 nm	74.4 %	56.5 %	21.7 %	3.3 %
700 nm	50.2 %	67.5 %	25.9 %	3.7 %

Table 4. Uncertainties of the input parameters for the model, given in terms of one standard deviation.

Parameter	Standard deviation (%)
$D_{p,\text{TDMPS}}$	1.1
$D_{p,\text{APS}}$	3
$N_{\text{TDMPS},3-20\ nm}$	10
$N_{\text{TDMPS},20-200\ nm}$	3.3
$N_{\text{TDMPS},200-700\ nm}$	8.3
N_{APS}	3.3
BC mass concentration	4
BC density	11
n_{non}	0.5
n_{BC}	4
i_{non}	0
i_{BC}	6.6

ancies probably stem from the uncertainties of the measurements and models, which have not been taken into account. Analysis of uncertainties is needed for such comparison.

4.2.2 Uncertainties of dry aerosol optical closure

To estimate the influence of the uncertainties in the model input parameters on the calculated σ_{sp} and σ_{bsp}, a Monte Carlo simulation was applied for both spring and summer datasets. The simulation repeatedly used a set of randomly varied input parameters with normally distributed frequency.

Uncertainties of measurements

The model input parameters used in the dry aerosol optical closure are listed in Table 4. For each parameter, the deviation is considered to conform to a normal distribution. The original values of model input parameters mentioned in Sect. 3 are applied as the mean values. The standard deviations of the normal distributions for these values are listed in Table 4.

There are many factors influencing the uncertainties in number concentration and particle size, including CPC, UCPC, APS and DMA measurement uncertainties. The TDMPS measurement induces uncertainties in both size and

Table 5. Mean standard deviations of the calculated σ_{sp} and σ_{bsp} yielded from the Monte Carlo simulation.

| | Standard deviation of σ_{sp} (%) | | | | Standard deviation of σ_{bsp} (%) | | | |
| | spring | | summer | | spring | | summer | |
λ	external	internal	external	internal	external	internal	external	internal
450 nm	8.25	9.19	8.38	9.49	7.28	8.48	7.83	9.54
550 nm	8.23	8.94	8.36	9.14	7.23	8.17	7.73	8.99
700 nm	7.87	8.35	8.13	8.62	7.16	7.80	7.60	8.40

Table 6. The ratios of the amount of nephelometer-measured σ_{sp} and σ_{bsp} fall within the range of the corresponding calculated values based on the assumptions of internal and external mixture to the total amount of the measured values, considering the uncertainties of the calculations.

| | σ_{sp} | | σ_{bsp} | |
λ	spring	summer	spring	summer
450 nm	99.71 %	98.57 %	87.20 %	61.47 %
550 nm	99.57 %	98.71 %	88.77 %	80.05 %
700 nm	99.51 %	98.99 %	90.58 %	65.10 %

number concentration. From a comparison test reported by Wiedensohler et al. (2010), the uncertainty of $D_{p,\text{TDMPS}}$ is estimated to be 3.5 %, and the uncertainties of N_{TDMPS} are estimated at 30 %, 10 % and 25 % for the size of 3–20 nm, 20–200 nm and 200–700 nm, respectively. The APS measurement induces uncertainties of 9 % and 10 % in size and number concentration, respectively (Wex et al., 2002). The uncertainty in BC mass concentration measured by MAAP is estimated as 12 %, as reported by Petzold et al. (2004). It should be noted that OC may also have light-absorbing components, such as HUmic-LIke Substances (HULIS) (Graber et al., 2006), thus causes a bias in the BC mass concentration reported by MAAP. This possible source of uncertainty is not considered in this study. In open literatures, BC density is reported from 1.00 to 2.00 g/cm^3 (Sloane et al., 1983, 1984; Sloane and Wolff, 1985; Sloane et al., 1991; Ouimette and Flagan, 1982; Seinfeld and Pandis, 1998). The standard deviation of BC density is constrained to cover the above mentioned range. Similarly, the standard deviation for the refractive indices is also chosen to agree with the values reported in open literatures (Ouimette and Flagan, 1982; Sloane, 1984; Seinfeld and Pandis, 1998; Covert et al., 1990). The uncertainty of measured σ_{sp} and σ_{bsp} is estimated at 10 % (Anderson et al., 1998; Heintzenberg et al., 2006).

Monte Carlo variations

A Monte Carlo simulation was applied to obtain the uncertainties of the results introduced by the uncertainties of the

Mie model input parameters. Mie calculations were repeated with each data record of the measurements, using a randomly varying set of input parameters. The random values of input parameters were chosen according to Table 4, and distributed as normal distributions. Several hundreds of runs were done for each of the 3492 data records in spring and 3553 data records in summer to obtain the standard deviation of the σ_{sp} and σ_{bsp} at all the three wavelengths, for both external and internal mixture.

Table 5 summarizes the mean standard deviations of the calculated σ_{sp} and σ_{bsp} derived from the Monte Carlo simulation. It can be found that the standard deviations of calculated σ_{sp} and σ_{bsp} are around 8 %. For a normal distribution, the range of mean value plus/minus triple standard deviation covers 99 % of all possible values. Thus, the uncertainties of the Mie model results are equal to the values of triple standard deviation. The uncertainties of the calculated σ_{sp} and σ_{bsp} are approximately within ±30 %.

Comparisons similar to those described in Sect. 4.2.1 were carried out for the measured and calculated values, taking into account the uncertainties. For σ_{sp} and σ_{bsp}, the calculated value with assumption of external mixture plus triple standard deviation and the calculated value with assumption of internal mixture minus triple standard deviation were defined as the boundaries of the possible range within which the measured value should be fall.

Table 6 displays the ratio of the amount of measured σ_{sp} and σ_{bsp} which fall within the possible range to the total amount of measured σ_{sp} and σ_{bsp}. For all the three wavelengths, more than 97 % of the measured σ_{sp} fall within the possible range of Mie calculations for both spring and summer. For σ_{bsp}, the ratios of points that fall within the possible range are lower than those for σ_{sp}.

The results of the closure comparison for backscattering are not as good as for total scattering. A possible reason is that compared with total scattering, the backscattering is probably more sensitive to the shape of the particles. Non-spherical particles may cause higher backscattering than spherical ones. An indirect evidence is that high backscattering ratio (b) was observed during dust event in HaChi campaign. Dust particles have non-spherical shape and make significant contribution to aerosol optical properties during dust event. Therefore, with the assumption of

spherical shape for all particles, the Mie calculation will underestimate the backscattering.

Considering the uncertainties, most of the measured σ_{sp} and σ_{bsp} agree with the calculated values. However, the uncertainties for the calculated σ_{sp} and σ_{bsp} are approximately $\pm 30\%$. This is mainly due to the large uncertainties of the Mie model input parameters. To reduce such uncertainties of calculation results, effort should be made to further improve measurement techniques to minimize the uncertainties of measured parameters. And more high quality measurements of aerosol chemical compositions are required to reduce the uncertainties in aerosol refractive indices.

5 Summary and conclusions

In early spring and summer of 2009, two field campaigns of aerosol physical properties were carried out in Wuqing, Tianjin in the NCP. In this investigation, we analyzed aerosol optical properties and conducted an optical closure experiment to examine the measurements and evaluate the uncertainties of measured parameters. The mean values of the measured σ_{sp} are 280 ± 253 and $379\pm251\,\mathrm{Mm^{-1}}$ at 550 nm in spring and summer, respectively. These values are lower than those measured in the urban area of Beijing (Bergin et al., 2001), similar to those measured in Yufa (Garland et al., 2009) and twice as much as that measured in SDZ (Yan et al., 2008). The mean values of the σ_{ap} during the two periods are 47 ± 38 and $43\pm27\,\mathrm{Mm^{-1}}$, respectively. They are only a half of those measured in Beijing urban area (Bergin et al., 2001), slightly lower than those measured in Yufa (Garland et al., 2009) and three times as much as those measured in SDZ (Yan et al., 2008). Overall, the σ_{sp} and σ_{ap} in Wuqing are higher than those in the regional areas of the NCP and are lower than those measured in urban of Beijing. The average ω values of dry aerosols at the wavelength of 637 nm are 0.82 ± 0.05 for spring and 0.86 ± 0.05 for summer. Three and two episodes with increased levels of pollution were observed in spring and summer campaign, respectively.

For the several aerosol parameters studied, pronounced and different diurnal cycles are found. The maximum value of the σ_{sp} and σ_{ap} appears at 06:00 LT–08:00 LT, and begins to decrease at 08:00 LT. A minimum is reached around 16:00 LT. During the night, the σ_{sp} and σ_{ap} remain at relative high values. This diurnal pattern is mainly influenced by the diurnal variation of the boundary layer height and direct particle emissions. The ω diurnal pattern shows two dips in the morning and evening probably caused by the truck emissions. The maximum ω occurs in the afternoon due to secondary aerosol formation and aging processes.

Aerosol optical properties are also highly related to the meteorological parameters. The average σ_{sp} and σ_{ap} for southerly winds are higher than for northerly winds caused by the significant transport of pollutants from southern regions. In spring, the maximum σ_{sp} and σ_{ap} occurred during periods with calm winds indicating the accumulation of local particle emissions. In summer, the maximum σ_{sp} and σ_{ap} occurred with southerly winds relating to the pollutants transport from southern areas. The ω accompanied by calm winds is always lower than that with higher wind speeds indicating a high fraction of BC in the locally emitted aerosols. The average ω for southerly winds is lower than that for northerly winds, because of the higher emission rates of BC in the southern areas of the NCP.

An aerosol optical closure experiment was applied for both of spring and summer measurements. Measured σ_{sp} and σ_{bsp} were compared with the corresponding calculated values obtained via a modified Mie model. The calculations were based on measured PNSDs and estimated refractive indices. A two-component optical aerosol model was assumed in the calculations. The σ_{sp} and σ_{bsp} were calculated separately under assumptions of internal mixture and external mixture of aerosols. Additionally, a Monte Carlo simulation was used to estimate the dependence of the σ_{sp} and σ_{bsp} calculation uncertainties on the uncertainties of input parameters used in the Mie model.

Good correlations are found between measured and calculated σ_{sp} and σ_{bsp} with R>0.98, confirming a stable performance of instruments. Considering the uncertainties of all input parameters used in the Mie model, the Monte Carlo simulation shows standard deviations of around 8% with uncertainties within 30% for the calculated σ_{sp} and σ_{bsp}. More than 97% of measured σ_{sp} at all the three wavelengths fall within the 99% confidence range of the calculated values, taking into account of the uncertainties of measured and calculated values. This indicates that the modified Mie model and corresponding assumptions used for the optical closure study are appropriate for estimating the aerosol optical properties.

References

Anderson, T. L. and Ogren, J. A.: Determining aerosol radiative properties using the TSI 3563 Integrating Nephelometer, Aerosol Sci. Technol., 29, 57–69, 1998.

Anderson, T. L., Covert, D. S., Marshall, S. F., Laucks, M. L., Charlson, R. J., Waggoner, A. P., Ogren, J. A., Caldow, R., Holm, R. L., Quant, G., Sem, J., Wiedensohler, A., Ahlquist, N. A., Bates, T. S.: Performance characteristics of a High-sensitivity, three-wavelength total scatter/backscatter nephelometer, J. Atmos. Ocean. Technol., 13, 967–986, 1996.

Albrecht, B. A.: Aerosols, cloud microphysics, and fractional cloudiness, Science, 245, 1227–1230, 1989.

Bergin, M. H., Cass, G. R., Xu, J., Fang, C., Zeng, L. M., Yu, T., Salmon, L. G., Kiang, C. S., Tang, X. Y., Zhang, Y. H., and Chameides, W. L.: Aerosol radiative, physical, and chemical properties in Beijing during June 1999, J. Geophys. Res., 106(D16), 17969–17980, 2001.

Birmili, W., Stratmann, F., Wiedensohler, A.: Design of a DMA-based size spectrometer for a large particle size range and stable operation, J. Aerosol Sci., 30(4), 549–533, 1999.

Bohren, C. F., Huffman, D. R.: Absorption and Scattering of Light by Small Particles, John Wiley, Hoboken, NJ, USA, 477–482, 1983.

Bond, T. C., Charlson, R. J., and Heintzenberg, J.: Quantifying the emission of light-absorption particles: measurements tailored to climate studies, Geophy. Res. Lett., 25(3), 337–340, 1998.

Bond, T. C., Streets, D. G., Yarber, K. F., Nelson, S. M., Woo, J.-H., and Klimont, Z.: A technology-based global inventory of black and organic carbon emissions from combustion, J. Geophys. Res., 109, D14203, doi:10.1029/2003jd003697, 2004.

Chandra, S., Satheesh, S. K., Srinivasan, J.: Can the state of mixing of black carbon aerosols explain the mystery of 'excess' atmospheric absorption?, Geophys. Res. Lett., L19109, doi:10.1029/2004GL020662, 2004.

Charlson, R. J., Schwartz, S. E., Hales, J. M., Cess, R. D., Coakley, J. A., Jr., Hansen, J. E., and Hofmann, D. J.: Climate forcing by anthropogenic aerosols, Science, 255, 423–430, doi:10.1126/science.255.5043.423, 1992.

Cheng, Y. F.: Aerosol radiative properties at Xinken in Pearl River Delta of China: An observation based numerical study, Ph.D. Thesis, Peking University, 2007.

Cheng, Y. F., Eichler, H., Wiedensohler, A., Heintzenberg, J., Zhang, Y. H., Hu, M., Herrmann, H., Zeng, L. M., Liu, S., Gnauk, T., Brüggemann, E., and He, L. Y.: Mixing state of elemental carbon and non-light-absorbing aerosol components derived from in situ particle optical properties at Xinken in Pearl River Delta of China, J. Geophys. Res., 111, D20204, doi:10.1029/2005JD006929, 2006.

Cheng, Y. F., Wiedensohler, A., Eichler, H., Su, H., Gnauk, T., Brüggemann, E., Herrmann, H., Heintzenberg, J., Slanina, J., Tuch, T., Hu, M., and Zhang, Y. H.: Aerosol optical properties and related chemical apportionment at Xinken in Pearl River Delta of China, Atmos. Environ., 42, 6351–6372, 2008a.

Cheng, Y. F., Wiedensohler, A., Eichler, H., Heintzenberg, J., Tesche, M., Ansmann, A., Wendisch, M., Su, H., Althausen, D., Herrmann, H., Gnauk, T., Brüggemann, E., Hu, M., and Zhang, Y. H.: Relative humidity dependence of aerosol optical properties and direct radiative forcing in the surface boundary layer at Xinken in Pearl River Delta of China: An observation based numerical study, Atmos. Environ., 42, 6373–6397, 2008b.

Cheng, Y. F., Berghof, M., Garland, R. M., Wiedensohler, A., Wehner, B., Müller, T., Su, H., Zhang, Y. H., Achtert, P., Nowak, A., Pöschl, U., Zhu, T., Hu, M., and Zeng, L. M.: Influence of soot mixing state on aerosol light absorption and single scattering albedo during air mass aging at a polluted regional site in northeastern China, J. Geophys. Res., 114, D00G10, doi:10.1029/2008JD010883, 2009.

Cooke, W. F., Liousse, C., Cachier, H., and Feichter, J.: Construction of a 1×1 fossil fuel emission data set for carbona-

ceous aerosol and implementation and radiative impact in the ECHAM4 model, J. Geophys. Res., 104, 22137–22162, 1999.

Covert, D. S., Heintzenberg, J., Hansson, H. C.: Electro-optical detection of external mixtures in aerosols, Aerosol Sci. Technol., 12, 446–456, 1990.

DeCarlo, P. F., Slowik, J. G., Worsnop, D. R., Davidovits, P., and Jimenez, J. L.: Particle Morphology and Density Characterization by Combined Mobility and Aerodynamic Diameter Measurements. Part 1: Theory, Aerosol Sci. Technol., 38(12), 1185–1205, 2004.

Dubovik, O., Holben, B. N., Eck, T. F., Smirnov, A., Kaufman, Y. J., King, M. D., Tanre, D., and Slutsker, I.: Variability of absorption and optical properties of key aerosol types observed in worldwide locations, J. Atmos. Sci., 59, 590–608, 2002.

Garland, R. M., Schmid, O., Rose, D., Nowak, A., Achtert, P., Wiedensohler, A., Gunthe, S. S., Takegawa, N., Kita, K., Kondo, Y., Hu, M., Shao, M., Zeng, L. M., Zhu, T., Andreae, M. O., and Pöschl, U.: Aerosol optical properties observed during Campaign of Air Quality Research in Beijing 2006 (CAREBeijing-2006): Characteristic differences between the inflow and outflow of Beijing city air, J. Geophys. Res., 114, D00G04, doi:10.1029/2008JD010780, 2009.

Graber, E. R. and Rudich, Y.: Atmospheric HULIS: How humic-like are they? A comprehensive and critical review, Atmos. Chem. Phys., 6, 729–753, doi:10.5194/acp-6-729-2006, 2006.

Heintzenberg, J. and Charlson, R. J.: Design and applications of the integrating nephelometer: a review. J. Atmos. Ocean. Technol., 13, 987–1000, 1996.

Heintzenberg, J., Wiedensohler, A., Tuch, T. M., Covert, D. S., Sheridan, P., Ogren, J. A., Gras, J., Nessler, R., Kleefeld, C., Kalivitis, N., Aaltonen, V., Wilhelm, R. T., and Havlicek, M.: Intercomparsions and aerosol calibrations of 12 commercial integrating nephelometer of three manufacturers, J. Atmos. Ocean. Technol., 23, 902–914, 2006.

Höller, R., Ito, K., Tohno, S., and Kasahara, M.: Wavelength dependent aerosol single-scattering albedo: Measurements and model calculations for a coastal site near the Sea of Japan during ACEAsia, J. Geophys. Res., 108(D23), 8648, doi:10.1029/2002JD003250, 2003.

IPCC: Climate Change 2007 – The Physical Science Basis, edited by: Solomon, S., Cambridge University Press, New York, USA, 2007.

Jacobson, M. Z.: A physically-based treatment of elemental carbon optics: Implications ofr global direct forcing of aerosols, Geophys. Res. Lett., 27(2), 217–220, 2000.

Liu, P., Zhao, C., Zhang, Q., Deng, Z., Huang, M., Ma, X., and Tie, X.: Aircraft study of aerosol vertical distributions over Beijing and their optical properties, Tellus B, 61, 756–767, 2009.

Lu, Z., Streets, D. G., Zhang, Q., Wang, S., Carmichael, G. R., Cheng, Y. F., Wei, C., Chin, M., Diehl, T., Tan, Q.: Sulfur dioxide emissions in China and sulfur trends in East Asia since 2000, Atmos. Chem. Phys., 10, 6311–6331, doi:10.5194/acp-10-6311-2010, 2010.

Mie, G.: Beiträge zur optic trüber Medien speziell kolloidaler Metallösungen, Ann. Phys., 25, 377–445, 1908.

Ouimette, J. R. and Flagan, R. C.: The extinction coefficient of multicomponent aerosols, Atmos. Environ., 16, 2405–2419, 1982.

Pesava, P., Horvath, H., and Kasahara, M.: A local optical closure experiment in Vienna, Aerosol Science, 32, 1249–1267, 2001.

Petzold, A. and Schönlinner, M.: Multi-angle absorption photometry a new method for the measurement of aerosol light absorption and atmospheric black carbon, J. Aerosol Sci., 35, 421 – 441, 2004.

Quinn, P. K., Anderson, T. L., Bates, T. S., Dlugi, R., Heintzenberg, J., v. Hoyningen-Huene, W., Kulmala, M., Russell, P. B., and Swietlicki, E.: Closure in tropospheric aerosol-climate research: A review and future needs for addressing aerosol direct short-wave radiative forcing, Phys. Atmos., 69(4), 547–577, 1996.

Quinn, P. K. and Coffmann, D. J.: Local closure during the first aerosol characterization experiment (ACE 1): aerosol mass concentration and scattering and backscattering coefficients, J. Geophys. Res., 103(D13), 16575–16596, 1998.

Rosenfeld, D.: TRMM observed first direct evidence of smoke from forest fires inhibiting rainfall, Geophys. Res. Lett., 26(20), 3105–3180, 1999.

Rosenfeld, D.: Suppression of rain and snow by urban and industrial air pollution, Science, 287, 1793–1796, 2000.

Seinfeld, J., Pandis, S.: Atmospheric chemistry and physics: from air pollution to climate change, Wiley, Inc., New York, USA, p. 701 and p. 1118, 1998.

Sheridan, P. J., Delene, D. J., Ogren, J. A.: Four years of continuous surface aerosol measurements from the Department of Energy's Atmospheric Radiation Measurement Program Southern Great Plains Could and Radiation Testbed site, J. Geophys. Res., 106(D18), 20735–20747, 2001.

Sloane, C. S.: Optical properties of aerosols – Comparison of measurements with model calculations, Atmos. Environ., 17, 409–416, 1983.

Sloane, C. S.: Optical properties of aerosols of mixed composition, Atmos. Environ., 18, 871–878, 1984.

Sloane, C. S. and Wolff, G. T.: Prediction of ambient light scattering using a physical model responsive to relative humidity: Validation with measurements from Detroit, Atmos. Environ., 19, 669–680, 1985.

Sloane, C. S., Watson, J., Chow, J., Pritchett, L., Richards, L. W.: Size-segregated fine particle measurements by chemical species and their impact on visibility impairment in Denver, Atmos. Environ., Part A, 25, 1013–1024, 1991.

Stratmann, F. and A. Wiedensohler.: A new data inversion algorithm for DMPS-measurements, J. Aerosol Sci., 27, suppl., 1, 339–340, 1996.

Street, D. G., Gupta, S., Waldhoff, S. T., Wang, M. Q., Bond, T. C., and Bo, Y.: Black carbon emission in China, Atmos. Environ., 35, 4281–4296, 2001.

Takemura, T., Nakajima, T., Dubovik, O., Holben, B. N., Kinne, S.: Single scattering albedo and radiative forcing of various aerosol species with a global three dimensional model, J. Climate, 15, 333–352, 2002.

Tuch, T. M., Haudek, A., Muller, T., Nowak, A., Wex, H., and Wiedensohler, A.: Design and performance of an automatic regenerating adsorption aerosol dryer for continuous operation at monitoring sites, Atmos. Meas. Tech., 2, 417–422, doi:10.5194/amt-2-417-2009, 2009.

Twomey, S.: Pollution and the planetary albedo, Atmos. Environ., 8, 1251–1256, 1974.

van Donkelaar, A., Martin, R. V., Brauer, M., Kahn, R., Levy, R., Verduzco, C., and Villeneuve, P. J.: Global estimates of ambient fine particulate matter concentrations from satellite-based

aerosol optical depth: Development and application, Environ. Health Perspect., 118, 847–855, 2010.

Wehner, B., Birmili, W., Ditas, F., Wu, Z., Hu, M., Liu, X., Mao, J., Sugimoto, N. and Wiedensohler, A.: Relationships between submicrometer particulate air pollution and air mass history in Beijing, China, 2004–2006, Atmos. Chem. Phys., 8, 6155–6168, 2008

Wex, H.: Closure and sensitivity studies on physical parameters of rural continental aerosols. Ph.D. Thesis, Leipzig University, 2002.

Wex, H., Neusüß, C., Wendisch, M., Stratmann, F., Koziar, C., Keil, A., Wiedensohler, A., Ebert, M.: Particle scattering, backscattering, and absorption coefficients: An in situ closure and sensitivity study, J. Geophys. Res., 107(D21), 8122, doi:10.1029/2000JD000234, 2002.

Wiedensohler, A., Orsini, D., Covert, D. S., Coffmann, D., Cantrell, W., Havlicek, M., Brechtel, F. J., Russell, L. M., Weber, R. J., Gras, J., Hudson, J. G., Litchy, M.: Intercomparsion study of the size-dependent counting efficiency of 26 condensation particle counters, Aerosol Sci. Technol., 27, 224–242, 1997.

Wiedensohler, A., Cheng, Y. F., Nowak, A., Wehner, B., Achtert, P., Berghof, M., Birmili, W., Wu, Z. J., Hu, M., Zhu, T., Takegawa, N., Kita, K. Kondo, Y., Lou, S. R., Hofzumahaus, A., Holland, F., Wahner, A., Gunthe, S. S., Rose, D., Su, H., and Pöschl, U.: Rapid aerosol particle growth and increase of cloud condensation nucleus activity by secondary aerosol formation and condensation: A case study for regional air pollution in northeastern China, J. Geophys. Res., 114, D00G08, doi:10.1029/2008JD010884, 2009.

Wiedensohler, A., Birmili, W., Nowak, A., Sonntag, A., Weinhold, K., Merkel, M., Wehner, B., Tuch, T., Pfeifer, S., Fiebig, M., Fjraa, A. M., Asmi, E., Sellegri, K., Depuy, R., Venzac, H., Villani, P., Laj, P., Aalto, P., Ogren, J. A., Swietlicki, E., Roldin, P., Williams, P., Quincey, P., Hüglin, C., Fierz-Schmidhauser, R., Gysel, M., Weingartner, E., Riccobono, F., Santos, S., Grning, C., Faloon, K., Beddows, D., Harrison, R. M., Monahan, C., Jennings, S. G., O'Dowd, C. D., Marinoni, A., Horn, H.-G., Keck, L., Jiang, J., Scheckman, J., McMurry, P. H., Deng, Z. Z., Zhao, C. S., Moerman, M., Henzing, B., and de Leeuw, G.: Particle mobility size spectrometers: harmonization of technical standards and data structure to facilitate high quality long-term observations of atmospheric particle number size distributions, Atmos. Meas. Tech. Discuss., 3, 5521–5587, doi:10.5194/amtd-3-5521-2010, 2010.

Wu, Z. J., Hu, M., Liu, S., Wehner, B., Bauer, S., Maßling, A., Wiedensohler, A., Petäjä, T., Dal Maso, M., and Kulmala, M.: New particle formation in Beijing, China: statistical analysis of a 1-year data set, J. Geophys. Res, 112, D09209, doi:10.1029/2006JD007406, 2007.

Xu, J., Bergin, M. H., Yu, X., Liu, G., Zhao, J., Marrico, C. M., and Baumann, K.: Measurement of aerosol chemical, physical, and radiative properties in the Yangtze delta region of China, Atmos. Environ., 36, 161–173, 2002.

Xu, J., Bergin, M. H., Greenwald, R., Schauer, J. J., Shafer, M. M., Jaffrezo, J. L., and Aymoz, G.: Aerosol chemical, physical, and radiaitve characteristics near a desert source region of northern China during ACE-Asia, J. Geophys. Res., 109, D19S03, doi:10.1029/2003JD004239, 2004.

Yan, P., Tang, J., Huang, J., Mao, J. T., Zhou, X. J., Liu, Q., Wang,

Z. F., and Zhou, H. G.: The measurement of aerosol optical properties at a rural site in Northern China, Atmos. Chem. Phys., 8, 2229–2242, doi:10.5194/acp-8-2229-2008, 2008.

Zhang, Q., Streets, D. G., Carmichael, G. R., He, K. B., Huo, H., Kannari, A., Klimont, Z., Park, I. S., Reddy, S., Fu, J. S., Chen, D., Duan, L., Lei, Y., Wang, L. T., Yao, Z. L.: Asian emissions in 2006 for the NASA INTEX-B mission, Atmos. Chem. Phys., 9, 5131–5153, doi:10.5194/acp-9-5131-2009, 2009.